INFRARED THERMOGRAPHY TO EVALUATE IMPACT DAMAGING OF COMPOSITES

C. Meola*, S. Boccardi, N.D. Boffa, F. Ricci, G.M. Carlomagno

Department of Industrial Engineering - Aerospace Division, University of Naples Federico II, Via Claudio, 21, 80125 Napoli, Italy

**carmeola@unina.it*

Keywords: Composites, impact tests, nondestructive evaluation, infrared thermography.

Abstract

This work would bear witness for the advantages of using infrared thermography to investigate the impact damaging of composites. To this end, different types of composites are used involving change of either the reinforcement (carbon, or glass fibers), or the matrix (thermoset, or thermoplastic). In particular, infrared thermography is used with a twofold function: as surface thermal mapping when the composite surface is being impacted and as non destructive evaluation technique before and after impact. The obtained results show that monitoring the thermal signatures induced by the impact supplies useful information for the material characterization, specifically for identifying origination and propagation of the impact damage which is useful for design purposes. The phase images, obtained with lockin thermography during nondestructive testing, allows for estimation of the damage extension, through the thickness and in plane, for preventative measures.

1. Introduction

Composite materials are increasingly used in an ever more wide number of applications such as in the transport industry, in civil infrastructures, in chemical equipments, as well in the fabrication of many objects for use in daily life. Their success is mainly due to their high strength-to-weight ratio, easy formability, and other properties that make them preferable to metals and other conventional engineering materials.

The mostly used composites include a polymeric matrix reinforced with fibers like carbon, or glass, which are generally referred to as fiber reinforced polymers (FRP). The development of composites started early in 1960 driven by requirements of the aeronautical sector leading mainly to the use of thermoset polymers as matrix because of their low density (low weight) [1]. In general, the fabrication of composites involves plies of fibers impregnated with epoxy resin [2] overlaid, owing to a fixed stacking sequence, and cured in autoclave. Fibrous composites have been used first for a variety of secondary wing and tail components [3] such as rudder and wing trailing edge panels [4]. The 2000s introduced a major breakthrough with the production of large passenger aircraft in which composites have been deployed extensively in primary load carrying structure with fuel saving and reduced CO_2 emission [5].

Since the first applications, composites exhibit different problems, when compared to metallic materials, in terms of type and occurrence of flaws from their production to their in-service

life. A main weakness of all the fiber reinforced thermoset polymers is their low interlaminar strength, which makes them susceptible to delamination under impact load [6]. The introduction, nowadays, of composites in other transport sectors, like the automotive, naval and railways, for which the lightness is not as imperative as in airplane, has driven the research interest also towards the use of thermoplastic matrices.

Actually, to maximize the composite toughness, thermoplastic matrices are the most promising; in fact, they are characterized by higher damage tolerance and interlaminar toughness, which is due to the presence of the amorphous phase that can limit the crack propagation and allow larger deformations [7]. Thermoplastic matrices also show advantages over the thermoset ones in terms of: potential recyclability after life-cycle, reprocessing, chemical and environmental resistance, reduced moisture absorption and, usually, faster production as well as reduced processes costs [8]. In addition, a good-to-impact performance material can be tailored by managing interface strength; in fact, the interface strength between fibers and matrix plays a key role in dissipating energy during an impact [9].

Besides the many advantages, composites pose also some problems in terms of establishing duration and fatigue-life criteria. In fact, the duration of a metallic component is dependent on the possible formation of cracks and their growth. Metal fracture mechanics is often adequate to predict the size of critical flaws and, as a consequence, to establish rejection/acceptance criteria on the basis of the designer requirements. On the contrary, composites are broadly inhomogeneous and behave in a complex way which is difficult to be modeled. In fact, a lot of models have been developed to describe the variety of possible defects such as interlaminar debonding, matrix degradation, fiber rupture and total or partial separation between matrix and fibers [10]. At the moment, all these models seem to be unable to completely describe the complexity of the starting point of the failure and its propagation in composites so that, the availability of experimental data is of great importance.

In this context, infrared thermography represents a useful investigation tool. Indeed, infrared thermography proved already its usefulness within a two-fold objective of surface thermal mapping when the specimen is being impacted and as non destructive evaluation (NDE) technique [11÷13]. In particular, Meola and Carlomagno [11] supplied information on onset and propagation of impact damage in glass fibers reinforced polymers (GFRP) through the analysis of thermoplastic effects. Recently, they demonstrated the important role played by manufacturing defects, like porosity and fibers misalignment, in the behavior of GFRP to impact load [13]. Infrared thermography proved also suitability to establish the impact energy value for the onset of damage in carbon fiber reinforced polymers (CFRP), which agrees with the acoustic emission recorded by piezo-patches [12]. It is worth noting that in the previously mentioned works [11÷13] the material matrix was a thermoset one.

The intention of the present work is to demonstrate the capability of an infrared imaging device to deal with two main types of information which are of great relevance for both development and use of composite materials. One regards the onset and propagation of impact damage, which are recorded online while the material undergoes impact; this is mainly important for design purposes. The other one is linked to the possibility to detect delamination, induced by an impact, at an early stage for preventative measures. The ability of infrared thermography is assessed through its use with different types of composites involving variation of both the type of matrix (from a thermoset to a thermoplastic one) and the type of reinforcement (from carbon to glass) to encompass many different deployments of composite materials.

2. Experimental tests

2.1. Description of specimens

Three different types of specimens are considered:

- The first type includes a thermoset (epoxy resin) matrix reinforced with carbon fibers following the stacking sequence $[0,45,90\text{-}45]_s$. More specifically, unidirectional carbon fibers impregnated with epoxy resin are overlaid by the hand lay-up technology and cured in autoclave. Specimens are 150x100 mm^2, 2.4 mm thick and are named $CFRP_{ts}$.

- The second type includes again a thermoset (epoxy resin) matrix, but reinforced with glass fibers following the stacking sequence $[0_2,90_2]_s$. Again the hand lay-up technology is used, but with curing under press at ambient temperature. Specimens are 130x100 mm^2, 2.9 mm thick and are named $GFRP_{ts}$.

- The last type of specimens involves again glass fibers, but embedded in a thermoplastic propylene matrix. Again the lay-up technology is used to overlay layers of glass fabric and polypropylene, but with curing in a compression molding machine. Specimens are 230x230 mm^2, 3 mm thick and are named $GFRP_{tp}$.

2.2. Test setup and procedure

All specimens are first non-destructively inspected with lock-in thermography to search for any manufacturing defects. Then, each specimen is impacted at a fixed energy on one side while the infrared camera views its rear side. Finally, each impacted specimen is inspected again with lock-in thermography to find out damage likely occurred during impact.

The used infrared camera is the SC6000 (Flir systems), which is equipped with a QWIP detector working in the 8-9 μm infrared band, has a 50 mm focal length lens, a spatial resolution 640x512 pixels full frame and a windowing option linked to frequency frame rate and temperature range. The same camera, equipped with the Lock-in option and the IrNDT® software, is used for non-destructive tests [13]. The setup for lockin non-destructive tests includes the specimen, the infrared camera and a halogen lamp for thermal stimulation of the specimen. More specifically, the infrared camera is equipped with a Lock-in module that drives the halogen lamp to generate a thermal wave of selectable frequency *f*.

The thermal wave, delivered to the specimen surface, propagates inside the material and gets reflected when it reaches parts where the heat propagation parameters change (in-homogeneities). The reflected wave interferes with the surface wave producing an oscillating interference pattern, which can be measured in terms of temperature amplitude, or phase angle ϕ, and represented, respectively, as amplitude, or phase, images. The basic link of the thermal diffusion length μ to the heating frequency *f* and to the material thermal diffusivity coefficient α is via the relationship:

$$\mu = \sqrt{\frac{\alpha}{\pi f}} \tag{1}$$

The depth range for the amplitude image is given by μ, while the maximum depth *p*, which can be reached for the phase image, corresponds to 1.8μ [14-16]. In general, it is preferable to

reduce data in terms of phase image because of its insensitivity to both non uniform heating and local variations of emissivity over the monitored surface. The material thickness, which can be inspected, depends on the wave period (the longer the period, the deeper the penetration) and on the material thermal diffusivity.

Impact tests are carried out with a modified Charpy pendulum, which allows enough room for positioning of the infrared camera to view the rear specimen surface (i.e., opposite to that struck by the hammer) [13]. Specimens are placed inside a special lodge which includes two larger plates with a window 15 cm x 7.5 cm to allow for the contact with the hammer from one side and optical view (by the infrared camera) from the other side. The hammer has hemispherical nose 12.7 mm in diameter. The impact energy E is set by suitably adjusting the falling height of the Charpy arm. Two values are herein considered E = 5 and 10 J. Sequences of thermal images are acquired at 96 Hz during impact tests. To allow for a complete visualization of thermal effects evolution with respect to the ambient temperature, the acquisition starts few seconds before the impact and lasts for some time after.

3. Data analysis

3.1. On-line surface temperature mapping

For impact tests, to better analyze the material's thermal behavior, the first image (t = 0 s) of the sequence, i.e. the specimen surface (ambient) temperature before the impact, is subtracted to each subsequent image so as to generate a map of temperature difference ΔT:

$$\Delta T = T(i,j,t) - T(i,j,0) \tag{2}$$

i and j representing lines and columns of the surface temperature map. Some examples of ΔT images are shown in the following figures 1-5 for the different specimens.

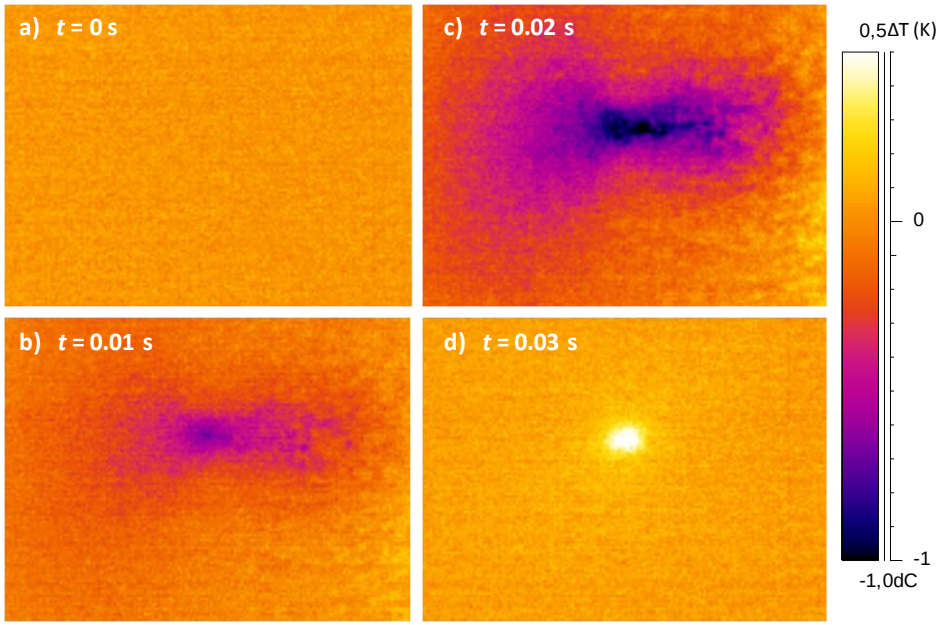

Figure 1. ΔT images of the $CFRP_{ts}$-1 for E = 5 J.

Fig.1 shows ΔT images of the $CFRP_{ts}$-1 specimen impacted with E = 5 J. The first image (Fig.1a) refers to the instant before the impact, which is assumed as t = 0 s; the specimen is at ambient temperature resulting in an almost uniform ΔT = 0 K. The successive images, taken

lately at t = 0.01 s (Fig.1b) and at t = 0.02 s (Fig.1c), display a central darker zone (negative ΔT values) accounting for thermo-elastic effects [11]. More lately, at t = 0.03 s (Fig.1d), a lighter hot zone appears accounting for dissipation of energy there. Indeed, the over-temperature variation is limited to a maximum value of about 0.5 K meaning that practically no important damage occurred. As the impact energy is increased to 10 J, the material undergoes more important damage as the thermal signature in Fig.2a proves. In fact, in this case, a hot oblong structure (about 11 mm long and 3 mm wide) appears sudden at the impact (t = 0.01 s) surrounded by a colder (dark) zone. This means that fibers break along their horizontal (longer side) direction while the remaining surface is in tension under the pushing impact force. On the other hand, there is an abrupt temperature rise (Fig.2a, ΔT = 20 K) accounting for fibers breakage. However, such a ΔT value is displayed only on a couple of images (i.e, fractions of a second) since there is a sudden cooling down towards the ambient temperature. More specifically, there is first a fast decrease followed by a slower one as the heat transfer rate is driven by the ΔT value. In particular, the ΔT decrease is accompanied by a better discrimination of the total extension of the warm zone; in fact, the maximum extension of equivalent diameter about 13 mm is visible for t = 1.79 s (Fig.2b). Such a warm zone may be assumed to coincide with the overall delaminated area [11, 13].

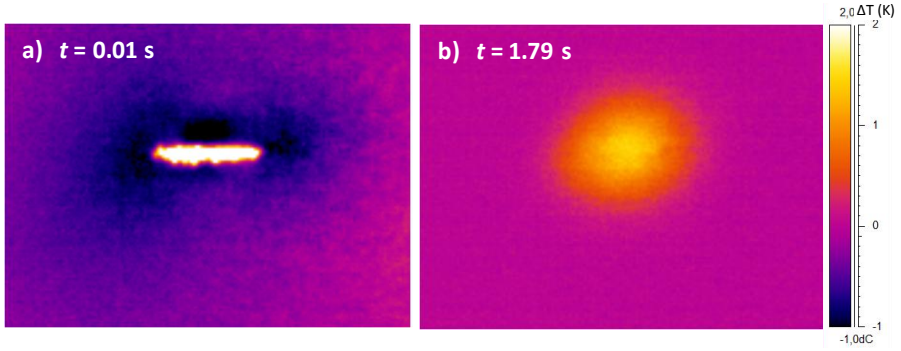

Figure 2. ΔT images of the $CFRP_{ts}$-2 for E = 10 J.

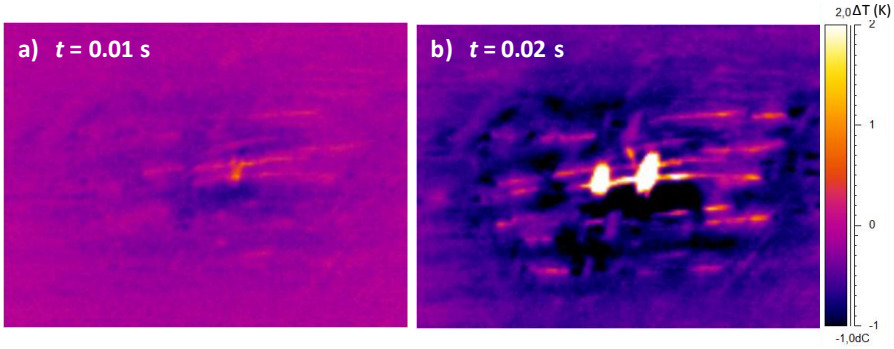

Figure 3. ΔT images of the $GFRP_{ts}$-1 for E = 5 J.

Figs.3 and 4 show ΔT images taken during impact respectively at E = 5 and 10 J of the $GFRP_{ts}$ specimens. As can be seen, a hot spot appears sudden at the impact with E = 5 J (Fig.3a) which at 0.02 s, strengthens up to ΔT = 31.6 K when a second lighter hot spot appears (Fig.3b) nearby on the left. Conversely, at the higher impact energy of E = 10 J, only one hot spot (ΔT = 24.2 K) appears for t = 0.02 s (Fig.4b and c). The location of such a hot spot can be recognized, from a comparison of Fig.4a with Fig.4b, in the junction of the vertical central fiber with the horizontal dark line (Fig.4a). The overall warm zone (delaminated area) is attained for t = 4.57 s when the maximum ΔT value jumps to 1.5 K (Fig.4d). From the latter image it is possible to distinguish, inside the whole warm zone (about 11x6 mm^2), a hotter

circular zone (ΔT = 1.5 K) of diameter 3 mm, which practically coincides with the hot spot of Fig.4b and c. Of course, this small area bears witness for the most important damage (fiber breakage), while outside, as $\Delta T \rightarrow 0$, delamination becomes much milder. From a comparison of Fig.4 with Fig.3, it is possible to see that the stronger hot spot in Fig.3a is located at the apex of a bifurcation within two fiber pockets and corresponds to the hammer head axis. It is just such a misalignment of fibers coupled with a non uniform distribution of resin that has favored the breakage of fibers and matrix with a great dissipation of energy and abrupt increase of temperature (ΔT = 31.6 K) for E = 5 J. In fact, it has already been demonstrated the detrimental effect of defects on the material performance under impact [13].

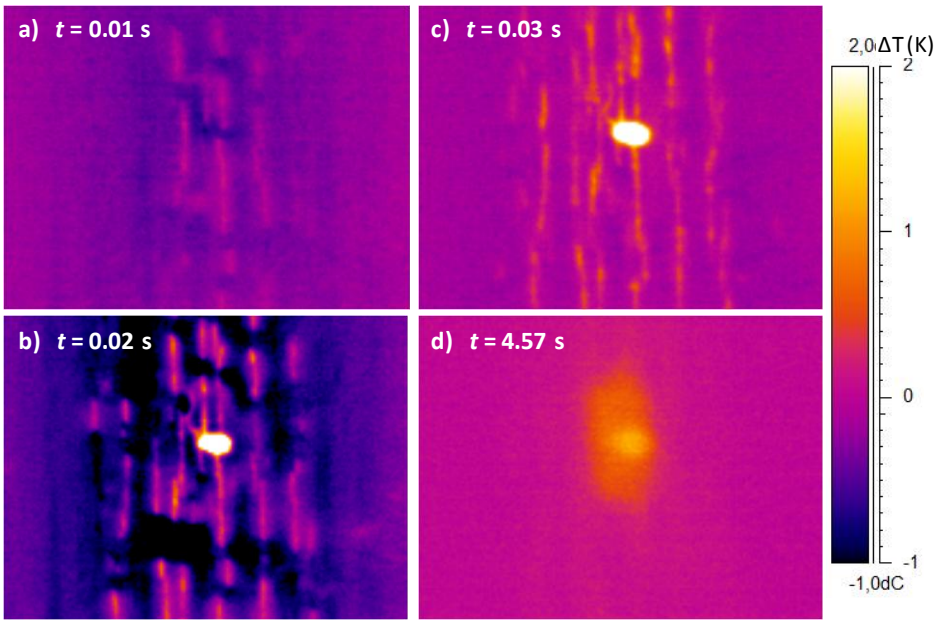

Figure 4. ΔT images of the $GFRP_{ts}$-2 for E = 10 J.

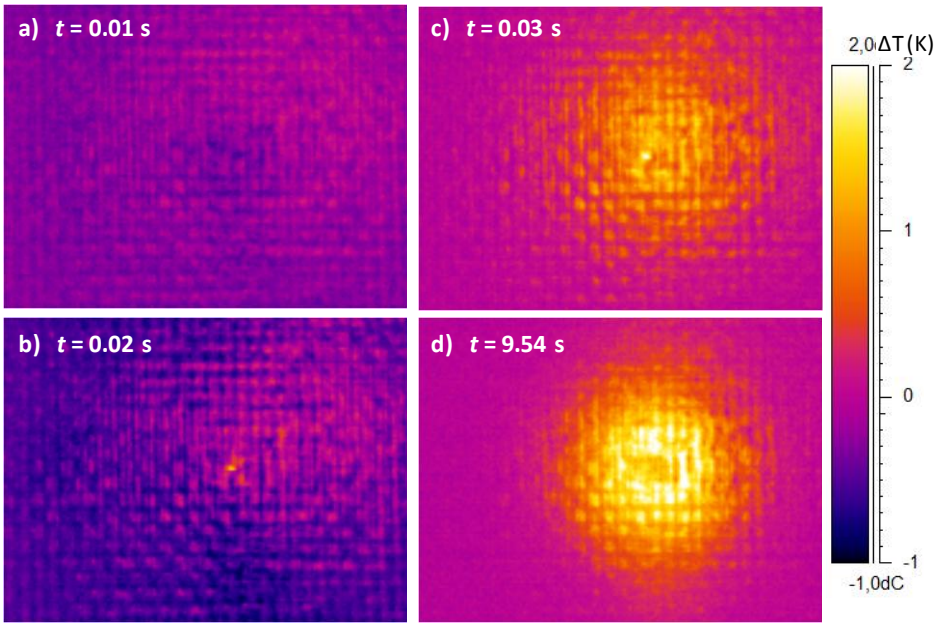

Figure 5. ΔT images of the $GFRP_{tp}$-2 for E = 10 J.

At last, some ΔT images, taken at different time instants, of a $GFRP_{tp}$ specimen impacted at E = 10 J are shown in Fig.5. A different behavior under impact is suddenly perceived for this

thermoplastic matrix based material. In fact, a much wide surface is affected by the thermo-elastic effect since the entire viewed surface cools down almost uniformly (Fig.5 a,b). The warm zone takes a circular shape (Fig.5c, d) of diameter about 20 mm with its center coinciding with the hammer head axis. The maximum ΔT attains a value of 2.3 K, which is much lower than the value (ΔT = 24.2 K) showed by the $GFRP_{ts}$ impacted at the same energy of E = 10 J and having the same thickness. In addition, unlike the thermoset matrix based specimens which show a sudden cooling down towards ambient temperature, the $GFRP_{tp}$ specimen displays a ΔT = 2.3 K which remains constant for long time, until over 9 s (Fig.5d). This behavior let to suppose debonding between matrix and fibers layers. It is apparent that the type of matrix and the type of bond between fibers and matrix play a key role in the behavior of the material under impact. In particular, the thermoplastic matrix seems to approach the behavior of metals, which react with a plastic deformation to the impact pushing force. On the other hand, unlike thermoset matrix based composites ($GFRP_{ts}$ and $CFRP_{ts}$), deformation, in the form of indentation and swelling, is visible, to the naked eye, over the $GFRP_{tp}$ specimen surface.

3.2. Non-destructive evaluation

Phase images of the three different materials, taken, from the side opposite to the impact of E = 10 J, at the same heating frequency of f = 0.2 Hz, are compared in Fig.6. Practically, in a thermoset matrix (Fig.6a, b) the damage starts from the rear side and develops along the main external fibers direction. Instead, in a thermoplastic matrix (Fig.6c) the material undergoes indentation and swelling in a circular shaped fashion according to the impactor geometry. From phase images it is also possible to follow the evolution of the impact damage through the thickness; of course, this is done starting from the impacted side and by decreasing the heating frequency (Eq.1). As an example, Fig.7 shows three phase images of the specimen $GFRP_{ts}$ -2 impacted with E = 10 J. As can be seen, the first image, taken for f = 0.88 Hz, displays only an indentation point, which is indicated by an arrow in Fig.7a. As the heating frequency decreases to 0.36 Hz (Fig.7b), a lighter zone may be distinguished (encircled in figure), which enlarges to a further decrease of f to 0.10 Hz (Fig.7 c); such a lighter zone accounts for local delamination. It is worth noting that the scale of Fig.6 and Fig.6 is not the same.

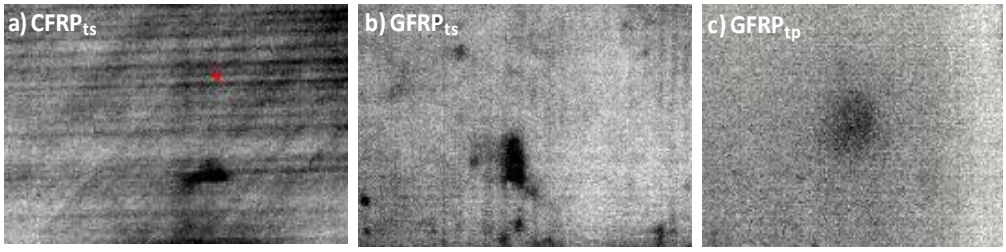

Figure 6. Phase images on the rear-to-impact side of specimens $CFRP_{ts}$-2, $GFRP_{ts}$-2 and $GFRP_{tp}$-2, for E = 10 J.

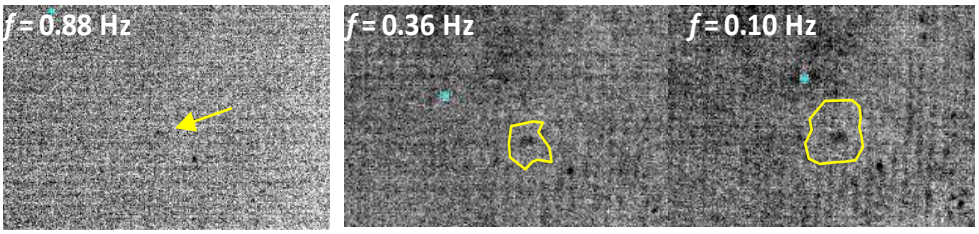

Figure 7. Phase images, taken at different heating frequencies, on the specimen $GFRP_{ts}$ -2 impacted at E = 10 J.

4. Conclusions

The results shown in this paper demonstrate the suitability of infrared thermography to both monitoring on line the thermal response to the impact and nondestructive evaluation after the impact of three different types of composites involving either a thermoset matrix (reinforced with either carbon, or glass fibers), or a thermoplastic matrix reinforced with glass fibers. In particular, recording the thermal signatures on the rear-to-impact side, helps to get useful hints about the material reaction to the impact, and the eventual damage generation and propagation. In fact, during the impact event, it is possible to visualize, depending on the type of matrix and fiber as well on the fibers orientation, any material damage occurred through the appearance of hot spots, lines, or circular structures. Nondestructive evaluation, performed, before and after impact, with the lockin technique, helps understanding abnormal reactions in presence of local defects. A joint examination of thermal images (recorded during the impact) and phase images (taken after the impact) allows gaining information on the overall delamination, which is important to assess the material performance.

References

[1] A. A. Baker, S. Dutton and D. Kelly. Composite Materials for Aircraft Structures, 2nd ed., *AIAA Education Series*, 2004.
[2] K. Urech, Liquid matrix system based on a mixture of epoxide resin and an amine curing agent for producing fibre-reinforced plastics components US Patent 4366108 (1982).
[3] R. Shütze, Aircraft wings US Patent 5496002 (1996)
[4] M. Piening, A. Pabsch and C. Sigle. Structural element of high unidirectional rigidity, US Patent 6355337, (2002)
[5] Key to metals, retrieved at http://www.keytometals.com/Article103.htm on Feb. 2014.
[6] S. Abrate. Impact on composite structures. Cambridge University Press, 1998.
[7] O. Çoban, M. Ö. Bora, T. Sinmazçelik, İ. Cürgül and V. Günay. Fracture morphology and deformation characteristics of repeatedly impacted thermoplastic matrix composites, *Materials & Design*, (30), 628–634, 2009.
[8] M. C. Collier and D. G. Baird. Separation of a thermotropic liquid crystalline polymer from polypropylene composites, *Polymer Composites*, (20), 423–435, 1999.
[9] P. Russo, D. Acierno, G. Simeoli, S. Iannace and L. Sorrentino. Flexural and impact response of woven glass fiber fabric/polypropylene composites, *Composites Part B: Engineering*, (54), 415–421, 2013.
[10] R. Krueger. Fracture mechanics for composites: State of the art and challenges retrieved at http://ntrs.nasa.gov/archive/nasa/casi.ntrs.nasa.gov/20080014103_2008013648.pdf on Feb. 2014.
[11] C. Meola and G. M. Carlomagno. Impact damage in GFRP: new insights with Infrared Thermography, *Composites Part A*, (41), 1839-1847, 2010.
[12] C. Meola, G. M. Carlomagno and F. Ricci. Monitoring of impact damage in Carbon Fibre Reinforced Polymers, in Proceedings QIRT 2012, paper n. 374, 8 pages, 2012.
[13] C. Meola and G. M. Carlomagno. Infrared thermography to evaluate impact damage in glass/epoxy with manufacturing defects, *Int. J. Impact Engineering*, (67), 1-11, 2014.
[14] A. Letho, J. Jaarinen, T. Tiusanen, M. Jokinen and M. Luukkala, Magnitude and phase in thermal wave imaging. *Electron. Lett.* (17), 364–365, 1981.
[15] C. A. Bennett Jr. and R. R. Patty, Thermal wave interferometry: a potential application of the photoacoustic effect. *Appl. Opt*. (21), 49–54, 1982.
[16] G. Busse, Optoacoustic phase angle measurement for probing a metal. *Appl. Phys. Lett*. (35), 759–760, 1979.